

Resonant quantum dynamics of few ultracold bosons in periodically driven finite lattices

S.I. Mistakidis,¹ T. Wulf,¹ A. Negretti,^{1,2} and P. Schmelcher^{1,2}

¹*Zentrum für Optische Quantentechnologien, Universität Hamburg,
Luruper Chaussee 149, 22761 Hamburg, Germany*

²*The Hamburg Centre for Ultrafast Imaging, Universität Hamburg,
Luruper Chaussee 149, 22761 Hamburg, Germany*

(Dated: September 20, 2018)

The out-of-equilibrium dynamics of finite ultracold bosonic ensembles in periodically driven one-dimensional optical lattices is investigated. Our study reveals that the driving enforces the bosons in different wells to oscillate in-phase and to exhibit a dipole-like mode. A wide range from weak-to-strong driving frequencies is covered and a resonance-like behaviour of the intra-well dynamics is discussed. In the proximity of the resonance a rich intraband excitation spectrum is observed. The single particle excitation mechanisms are studied in the framework of Floquet theory elucidating the role of the driving frequency. The impact of the interatomic repulsive interactions is examined in detail yielding a strong influence on the tunneling period and the excitation probabilities. Finally, the dependence of the resonance upon a variation of the tunable parameters of the optical lattice is examined. Our analysis is based on the ab-initio Multi-Configuration Time-Dependent Hartree Method for bosons.

Keywords: driving systems; non-equilibrium dynamics; shaken lattices; resonance; higher-band effects; inter-well tunneling; Floquet analysis; dipole mode; control dynamics; fidelity.

PACS numbers: 03.75.Lm, 67.85.Hj, 05.45.Mt, 05.60.Gg, 03.75.Kk

I. Introduction

Ultracold atomic quantum gases in optical lattices have reached an unprecedented degree of control providing direct experimental access to a plethora of non-equilibrium phenomena [1–4]. This control includes the modulation of the interparticle interactions via confinement-induced, magnetic and optical Feshbach resonances [5–10], the design of arbitrarily shaped optical traps with variable lattice depths, and the ability to move time-periodically or even accelerate the entire lattice structure. This level of control and accuracy over the system parameters has opened the possibility to simulate and study quantum many-body phenomena in part inspired from condensed matter physics [11]. For instance, when accelerating an optical lattice, representative processes are Bloch-oscillations [12–16], Wannier-Stark ladders [17, 18], Landau-Zener tunneling [16, 18] and photon assisted tunneling [19], to name only a few. A promising technique is the lattice shaking which has been used in order to address e.g., the coherent control of the superfluid to Mott insulator phase transition [20], parametric amplification of matter waves [21], four-wave mixing [22, 23], topological states of matter [24], hybridized band structure [21, 25], and even the engineering of artificial gauge fields [26]. More recently it has been shown [27, 28] that one can use lattice shaking to probe coherent band coupling and realize the formation of ferromagnetic domains. Moreover, the dynamics induced by shaking an optical lattice can lead to an admixture of excited orbitals [29] and constitutes an emergent branch of modern quantum physics.

A substantial part of the previous studies has been primarily focussing on the renormalization of the physics due to driving, the mean-field approach [14] for weak interactions, where the Gross-Pitaevskii equation is still valid, and a linear response treatment [30]. However, a relatively large modulation of the strength or of the frequency of the driving as well as strong interactions, calls for alternative methods which can take into account higher-orbitals. Indeed, the inclusion of higher-band contributions introduces new degrees of freedom and as a result additional physical processes come into play. Hereby, a sinusoidal shaking of the optical lattice is a natural starting point which induces an in-phase dipole mode on each site. An interesting and so far largely unexplored direction is the study of the interplay between higher bands for the intra-well mode and the inter-well tunneling dynamics with respect to the driving frequency, and the investigation of the effect of the interatomic interactions in the overall process. In this way, it is natural to start with the investigation of the few body analogue in order to achieve a more comprehensive understanding of the microscopic properties of the strongly driven interacting system. Although the major part of the presented results is devoted to the case of four bosons in a triple-well setup, we provide strong evidence that our findings are still applicable for larger lattice systems and larger particle numbers.

Motivated by the recent experimental progress [26, 27] we investigate in the present work the effects a periodically driven one-dimensional optical lattice can introduce in a small ensemble of ultracold bosons. The dynamical response of the system for a wide range of driving fre-

quencies is studied by means of the concept of fidelity or autocorrelation function. Even though we consider a scenario with a deep lattice such that the tunneling modes have a minor influence on the overall dynamics, a quite rich excitation spectrum is found. We note that such intra-band excitations, which lead to a coupling between the two lowest energy bands, have been exploited in order to realise single- and two-qubit gates, where the quantum bit has been encoded in the localised Wannier functions of the two lowest energy bands of each lattice site [31]. In order to analyze the intra-well dynamics we employ the one-body reduced density matrix. The Fourier spectrum of the local one-body density as well as of the on-site density oscillations are employed in order to obtain insights into the excited intra-well modes. We find a resonant behaviour of the dipole mode indicating that the intra-well dynamics can be controlled by adjusting the driving frequency. Moreover, the magnification of the intra-well generated mode at resonance is also manifested in the population of additional lattice momenta. Our investigation of the resonances is supported by a Floquet analysis for the effective single-particle degree of freedom. This allows us to further explore the on-site dynamics and the inter-well tunneling that occur due to the driving. Including interatomic interactions for larger atom numbers we analyze similarities and differences with respect to the single-particle description. The above outlined findings are confirmed for different filling factors, lattice potentials, and boundary conditions. To solve the underlying many-body Schrödinger equation we apply the *ab-initio* MultiConfiguration Time-Dependent Hartree method for Bosons (MCTDHB) [32, 33] which is especially designed to treat the driven out-of-equilibrium quantum dynamics of interacting bosons.

This article is organized as follows. In Sec. II we introduce our setup and the multi-band expansion. Sec. III contains the driven quantum dynamics first from a single-particle perspective, by performing a Floquet analysis, and second by inspecting the dynamics of a small bosonic ensemble including repulsive interactions. We summarize our findings and provide an outlook in Sec. V. Appendix A briefly outlines our computational method.

II. Hamiltonian and multi-band expansion

This section is devoted to a brief presentation of the theoretical framework of our study. In particular, we shall briefly discuss the driven optical lattice, the underlying many-body Hamiltonian, and the concept of multi-band expansion. The latter will be a useful tool in order to understand the excitations involved in the dynamics.

A. Modeling the periodically-driven potential

The periodic driving of an optical lattice can be accomplished in two different ways. Retroreflecting mirrors

that are used to form the lattice can be moved periodically in space or, alternatively, a frequency difference between counterpropagating laser beams can be induced by means of acousto-optical modulators [27] which renders the lattice time-dependent. Here, we model the driven optical lattice with a sinusoidal function of the form

$$V_{sh}(x, t) = V_0 \sin^2[k_0(x - A \sin \omega_D t)]. \quad (1)$$

Such a potential has been implemented in the experiment of e.g. ref. [21]. It is characterized by the barrier depth V_0 , a lattice wave-vector $k_0 = \frac{\pi}{l}$, where l denotes the distance between successive potential minima, the amplitude A and the frequency $\omega_D = 2\pi/T_D$ of the driving field. In an experiment k_0 is the wave vector of the laser beams which form the optical lattice, while its depth V_0 can be tuned by adjusting the lasers intensity.

B. The Hamiltonian

The Hamiltonian of N identical ultracold bosons of mass M confined in a driven one-dimensional m -well optical lattice reads

$$H = \sum_{i=1}^N -\frac{\hbar^2}{2M} \frac{\partial^2}{\partial x_i^2} + V_{sh}(x_i, t) + \sum_{i < j} V_{\text{int}}(x_i - x_j), \quad (2)$$

where $V_{\text{int}}(x_i - x_j) = g_{1D} \delta(x_i - x_j)$ denotes the short-range contact interaction potential between particles located at position x_i , $i = 1, 2, \dots, N$. In the ultracold regime the interaction is well described by s-wave scattering whose effective 1D coupling strength [5] is given by $g_{1D} = \frac{2\hbar^2 a_0}{M a_{\perp}^2} \left(1 - \frac{|\zeta(1/2)| a_0}{\sqrt{2} a_{\perp}}\right)^{-1}$. Here $a_{\perp} = \sqrt{\frac{\hbar}{M \omega_{\perp}}}$ is the transverse harmonic oscillator length with ω_{\perp} the frequency of the two-dimensional confinement, while a_0 denotes the free space 3D s-wave scattering length. In this way, the interaction strength can be tuned either via a_0 with the aid of Feshbach resonances [9, 10], or via the transversal confinement frequency ω_{\perp} [34, 35].

For the sake of simplicity and computational convenience, we rescale the Hamiltonian (2) in units of the recoil energy $E_R = \frac{\hbar^2 k_0^2}{2M}$. Then, the corresponding length, time and frequency scales are given in units of k_0^{-1} , $\omega_R^{-1} = \hbar E_R^{-1}$ and ω_R respectively. In our simulations we have used a sufficiently large lattice depth with values ranging from $V_0 = 4.5 E_R$ to $8.0 E_R$ such that each well includes three localized single-particle Wannier states. In particular, due to the deep optical lattice and small driving amplitudes (in comparison to the lattice constant) mainly used in our simulations highly energetic excitations above the barrier are excluded and as a consequence heating processes can be minimized. The confinement of the bosons in the m -well system is imposed by the use of hard-wall boundary conditions at positions $x_{\sigma} = \pm \frac{m\pi}{2k_0}$, where the potential is maximum. In addition, we set also $\hbar = M = k_0 = 1$ and the coupling strength becomes

$g = \frac{qV_D}{E_R}$, while A represents the dimensionless driving amplitude. The rescaled shaken triple well is given by $V_{sh}(x_i, t) = V_0 \sin^2(x_i - A \sin \omega_D t)$ with the hard wall boundaries located at $x_\sigma = \pm 3\pi/2$.

C. The multi-band expansion

The understanding of the spatial localization of states in lattice systems makes the use of multi-band Wannier number states crucial as it includes the information of excited bands and allows to interpret both intraband and interband processes. In general, this representation is valid when the lattice potential is deep enough such that the Wannier states between different wells have a very small overlap for not too high energetic excitation. In the present case where the potential is periodically driven the above description can still be used as long as the driving amplitude is small enough in comparison to the lattice constant l , i.e. $A \ll l$. In this way, each localized Wannier function can be still adapted and assigned to a certain well and the respective band-mixing is fairly small. For large displacements one should use a time-dependent Wannier basis in order to ensure that the corresponding on-site Wannier states are well-adapted to each well during the driving.

To introduce the formalism, let us consider a system consisting of N bosons, m -wells and k localized single particle bands [36, 37]. Then, the expansion of the many-body bosonic wavefunction in terms of the number states of non-interacting bosons reads

$$|\Psi\rangle = \sum_{\{N_i\}, \mathbf{I}} C_{\{N_i\}, \mathbf{I}} |N_1, N_2, \dots, N_m\rangle_{\mathbf{I}}, \quad (3)$$

where $|N_1, N_2, \dots, N_m\rangle_{\mathbf{I}}$ is the multiband Wannier number state and the element N_i denotes the number of bosons being localized in the i -th well satisfying the constraint $\sum_{i=1}^m N_i = N$. The summation is performed over the different configurations of the N bosons according to their energetical order denoted by the index \mathbf{I} . In particular, the index \mathbf{I} corresponds to a high dimensional quantity $\mathbf{I} = (I_1, I_2, \dots, I_m)$ which contains m elements each of them being a k -component vector. More precisely, the q -th element can be written as $I_q = (I_q^{(1)}, I_q^{(2)}, \dots, I_q^{(k)})$, where $I_q^{(k)}$ refers to the number of bosons located at the q -th well and k -th band, satisfying the constraint $\sum_{q=1}^m \sum_{i=1}^k I_q^{(i)} = N$. Within the above notation one can investigate, among others, the probability of $N_0 < N$ bosons to be in an excited band or to find a specific number state configuration. Indeed, suppose the case of $N_0 < N$ bosons excited in the i -th band while the rest $N - N_0$ lie in lower bands. Then, it must hold $I_1^{(j)} = I_2^{(j)} = \dots = I_m^{(j)} = 0$ for every $j > i$, while $I_1^{(i)} + I_2^{(i)} + \dots + I_m^{(i)} = N_0$ and $I_1^{(1)} + \dots + I_m^{(j_1)} = N - N_0$ for every $j_1 < i$.

Let us consider an example of a system with four bosons ($N = 4$) confined in a triple well ($m = 3$) which

includes three bands ($k = 3$). Then, for instance, the state $|1, 2, 1\rangle_{\mathbf{I}}$ with $\mathbf{I} = (I_L, I_M, I_R)$, and $I_L = I_R = (0, 1, 0)$, $I_M = (0, 1, 1)$ denotes a state for which in the left (right) well one boson occupies the first excited band, whereas in the middle well one boson is localized in the first excited and one in the second excited band. As a final attempt, here, we make a link between the ground state and its dominant spatial configuration in terms of the aforementioned multiband expansion. To do that, let us choose again a system consisting of four bosons in a triple well as it will extensively be used in the following. It is known that, in general, the ground state configuration depends on the interaction strength, while for the present system, i.e. $N = 4$ and $m = 3$, the on-site interaction effects will always be prominent. For the non-interacting case ($g = 0$) the dominant spatial configuration of the system is $|1, 2, 1\rangle_{\mathbf{I}}$, with $I_L = I_R = (1, 0, 0)$ and $I_M = (2, 0, 0)$ due to the hard-wall boundaries which render the middle and outer sites non-equivalent. In the course of increasing interaction a tendency towards a uniform population of each site, e.g. for $g = 0.2$, due to the repulsion of the bosons is observed. In this region the system is described by a superposition of lowest-band states which are predominantly of single-pair occupancy, e.g. $|1, 2, 1\rangle_{\mathbf{I}}$, $|2, 1, 1\rangle_{\mathbf{I}}$, and double-pair occupancy, e.g. $|2, 2, 0\rangle_{\mathbf{I}}$. For further increasing repulsion, e.g. $g = 0.4$, a trend towards the repopulation of the central well is noted. As we enter the strong interaction regime, e.g. $g = 1.5$, the state consists of a particle in the first excited-band being on a commensurate background of localized particles which lie in the zeroth band and the dominant ground state configuration is $|1, 2, 1\rangle_{\mathbf{I}}$, with $I_L = I_R = (1, 0, 0)$ and $I_M = (1, 1, 0)$. Finally, for strong interparticle repulsion, e.g. $g = 3$, the contribution from the higher-band states becomes more prominent and the corresponding ground state configuration is characterized by an admixture of zeroth- and excited-band states.

III. Driven quantum dynamics

This section is devoted to a detailed analysis of the bosonic dynamics in a driven optical lattice. At the beginning, a general overview of the effect of the driving on the finite bosonic ensemble with respect to the driving frequency is given. Subsequently, a Floquet analysis is employed in order to investigate the underlying single-particle physics. Finally, we focus on specific interaction effects.

A. Dynamical response

Let us explore the dynamical response or sensitivity of the system with respect to the driving frequency ω_D . In order to investigate the stability of the system against the perturbations induced by the shaking [see Eq.(1)], we first analyse the fidelity [38] between the initial state and

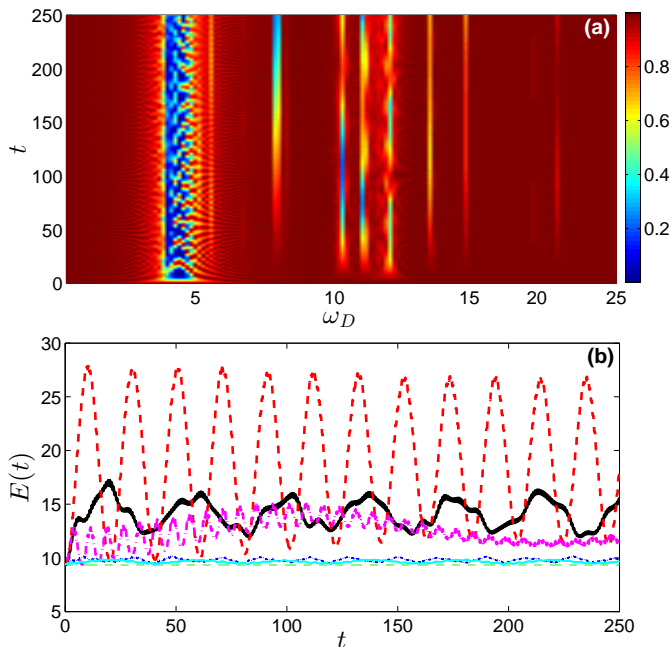


FIG. 1: (a) Time evolution of the fidelity $F_{\omega_D}(t)$ as a function of the driving frequency ω_D (measured in units of ω_R). (b) Time evolution of the expectation value of the Hamiltonian (2) (measured in units of the recoil energy E_R) for various driving frequencies $\omega_D = 0.4$ (green thin dashed line), $\omega_D = 4.0$ (black thick solid line), $\omega_D = 4.5$ (red thick dashed line), $\omega_D = 5.25$ (magenta thick dashed-dotted line), $\omega_D = 11.0$ (blue thin dashed-dotted line), and $\omega_D = 13.375$ (light-blue thin solid line). The driving amplitude is $A = 0.05$, while the initial state corresponds to the ground state of four weakly interacting bosons with $g = 0.1$ confined in a triple-well. Time unit is ω_R^{-1} .

the state evolved at time t : $F_{\omega_D}(t) = |\langle \Psi(0) | \Psi(t) \rangle|^2$, where the dependence on ω_D is implicit in the time evolved state $\Psi(t)$. Here we will consider a system of four bosons in a triple-well with $g = 0.1$, whose ground state (i.e., the initial state $\Psi(0)$) corresponds to a superfluid state, as the filling factor is not commensurable and we do not encounter the formation of a Mott insulating state. In terms of its dominant spatial configuration our system initially consists (see also Sec.II.C) of two bosons in the middle well and two others each of them localized in one of the outer wells, i.e. the state $|1, 2, 1\rangle_{\mathbf{I}}$, with $I_L = I_R = (1, 0, 0)$ and $I_M = (2, 0, 0)$ has the most prominent contribution. Figure 1(a) shows $F_{\omega_D}(t)$ as a function of the driving frequency ω_D . The dynamics is characterized by three main regions with respect to ω_D , where the system is driven far from the initial state, while for the remaining frequency regions (red sections in Fig. 1(a)) the evolved state is essentially unperturbed by the driving. In the first region, between $4.0 < \omega_D < 5.5$, the minimal overlap in the course of the dynamics drops down to 0.1, whereas in the second ($7.0 < \omega_D < 8.0$) and third ($10.0 < \omega_D < 15.0$) regions the system maxi-

mally departs from the initial state with a percentage on the order of 50% and 65%, respectively. The emergence of these dynamical regions strongly depends on the parameters of the optical lattice. For instance, for smaller lattice depths the aforementioned regions will be wider, because of the smaller potential energy, which favors a possible deviation of the system from the initial state.

Let us inspect the time evolution of the total energy $E(t) = \langle \Psi(t) | \hat{H}(t) | \Psi(t) \rangle$. Figure 1(b) shows $E(t)$ for various driving frequencies ω_D . For driving frequencies where $F_{\omega_D} \simeq 1$ [e.g. $\omega_D \in \{1, 3\}$, see also Fig. 1(a)] the dependence of the energy on the driving frequency is weak and it is essentially constant during the time evolution. On the other hand, for the regions where $F_{\omega_D} \ll 1$, $E(t)$ increases initially and it shows an oscillatory behaviour. In particular, for $\omega_D = 4.5$ the total energy exhibits an oscillatory (almost periodic) pattern which can also be observed in the corresponding fidelity evolution. This driving frequency will be referred to in the following as critical and denoted by ω_D^c , that is, the driving frequency for which $\min_{t \in [0, T]} F_{\omega_D}(t)$ is minimal. Indeed, as we shall see below, the most interesting dynamics of the system takes place close to this frequency.

Finally, let us inspect the response of the system to the driving from a one-body perspective via the single-particle density $\rho_1(x, t) = \int dx_2 \dots dx_N |\Psi(x, x_2, \dots, x_N; t)|^2$. Figure 2 illustrates the evolution of the one-body density for different driving frequencies ω_D , but with the same amplitude A . The driving leads to oscillations of the particles densities in every site. As it can be observed by having a glance at Fig. 2(a), the one-body density shows a weak response for driving frequencies away from the critical region $\omega_D \in [4, 5.5]$, while for $\omega_D = \omega_D^c$ [see Fig. 2(b)] we observe the periodic formation of enhanced density oscillations being accompanied by a broadening of each intra-well ensemble. The peculiar behaviour of the bosonic ensemble observed for $\omega_D = \omega_D^c$ is characterized by three processes and time scales: *i*) the internal fast oscillations of the density; *ii*) the large amplitude oscillations of the density in each well of period ~ 14 ; *iii*) the tunneling between the wells with a period of about 200. All these features will be analyzed in detail in the following subsections both at the single particle and many-body level.

B. Single particle dynamics

Here we investigate to which extent the previously presented results can be understood in the limit of zero interaction among the particles by means of Floquet theory. Specifically, we are interested in two distinct features of the dynamics observed in Fig. 2(b): First, the on-site dynamics and, especially, its resonance-like dependence on the driving frequency ω_D , and second, the inter-well tunneling dynamics which is enhanced at certain values of ω_D .

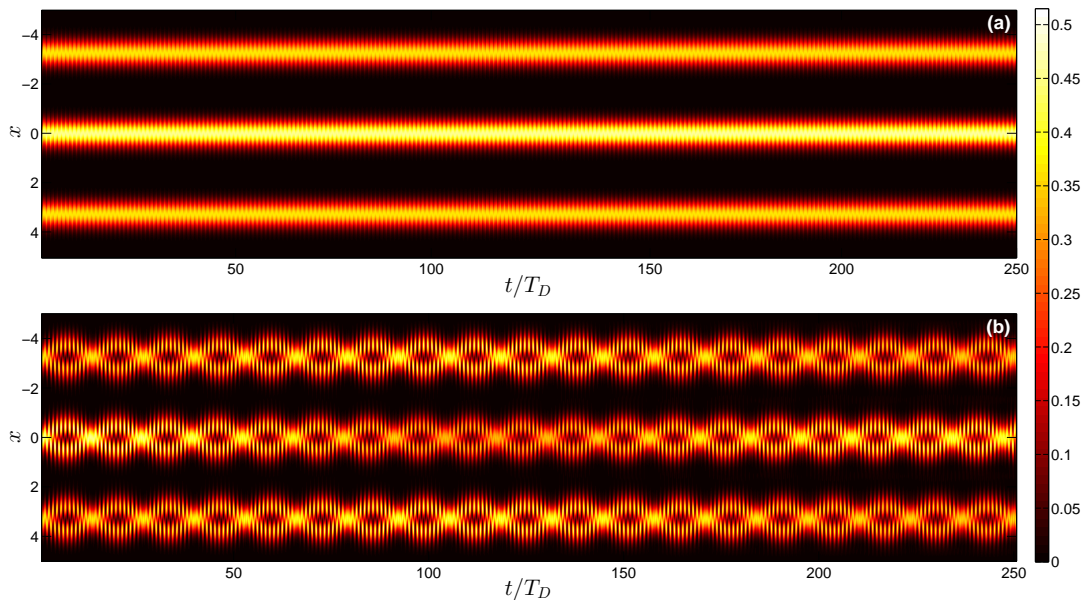


FIG. 2: Time evolution of the one-body density $\rho_1(x, t)$ in a triple-well potential for different driving frequencies: (a) $\omega_D = 2.0$ (top panel) and (b) $\omega_D = 4.5$ (lower panel). The driving amplitude is fixed to the value $A = 0.05$, while the initial state corresponds to the ground state of four weakly interacting bosons with $g = 0.1$. The spatial extent of the lattice is expressed in units of k_0^{-1} , while the time units are rescaled in terms of the driving period T_D .

1. Floquet theory

To be self-contained, we start by summing up the main notions of Floquet theory. Because of the temporal periodicity of the single particle Hamiltonian employed throughout this work [Eq. (2) with $g = 0$ and $N = 1$], every solution of the time-dependent Schrödinger equation (TDSE) takes the form of a Floquet mode (FM) $\Psi_\alpha(x, t)$ which in turn can be written as: $\Psi_\alpha(x, t) = e^{-i\epsilon_\alpha t/\hbar} \Phi_\alpha(x, t)$ with the real quasi energy (QE) $\epsilon_\alpha \in [-\hbar\omega_D/2, +\hbar\omega_D/2]$ and with $\Phi_\alpha(x, t) = \Phi_\alpha(x, t + T_D)$ respecting the temporal periodicity of the Hamiltonian [39]. The FMs are eigenvectors of the time evolution operator over one driving period

$$U(T_D + t_0, t_0)\Psi_\alpha(x, t_0) = e^{-i\epsilon_\alpha T_D/\hbar}\Psi_\alpha(x, t_0). \quad (4)$$

This property is of particular interest as it allows for a stroboscopic time evolution of an arbitrary initial state $\Psi(x, t_0)$ once the FMs of a system are known. To show this, we exploit the fact that the FMs constitute an orthonormal basis for the solution space of the TDSE [40] and expand $\Psi(x, t_0)$ at the initial time $t = t_0$ as

$$\Psi(x, t_0) = \sum_{\alpha} C_{\alpha}(t_0)\Psi_{\alpha}(x, t_0) \quad (5)$$

with the corresponding coefficients $C_{\alpha}(t_0)$. By applying the one period evolution operator $U(T_D + t_0, t_0)$ on both sides of Eq. (5) for m times and by virtue of Eq. (4), we readily obtain the stroboscopic time evolution of $\Psi(x, t_0)$

as

$$\Psi(x, t_0 + mT) = \sum_{\alpha} C_{\alpha}(t_0)e^{-i\epsilon_{\alpha}mT_D/\hbar}\Psi_{\alpha}(x, t_0). \quad (6)$$

Numerically, we obtain the FMs for a given initial time t_0 by calculating the eigenvectors of the one period evolution operator $U(T_D + t_0, t_0)$ [see Eq. (4)]. We refer the interested reader to ref. [41] for a detailed description of the employed computational scheme.

Finally, let us note that Eq. (6) already reveals some interesting features of the time evolution in periodically driven systems as we shall see in the following. Imagining that only a single FM, say $\Psi_0(x, t)$, is populated. The stroboscopic evolution of the probability density is thus given as $|\Psi(x, mT_D)|^2 = |C_0|^2|\Psi_0(x, 0)|^2$. Hence, $|\Psi(x, t)|^2$ is again periodic with period T_D and the only time dependence arises from the explicit time dependence of the FM, which is commonly referred to as "micro-motion". This situation changes if the initial state populates multiple FMs. In this case one encounters interference terms in $|\Psi(x, mT_D)|^2$ between the different FMs in the form of $\sim e^{im(\epsilon_{\alpha}-\epsilon_{\beta})T_D/\hbar}$. Thus, the quasi energies ϵ_{α} in periodically driven systems play a comparable role in the time evolution as the energy eigenvalues do in time independent setups.

2. On-site dynamics in the single well

To begin with, we shall investigate the observed on-site dynamics [see Fig. 2(b)], and in particular their dependence on the driving frequency ω_D . To this end, we

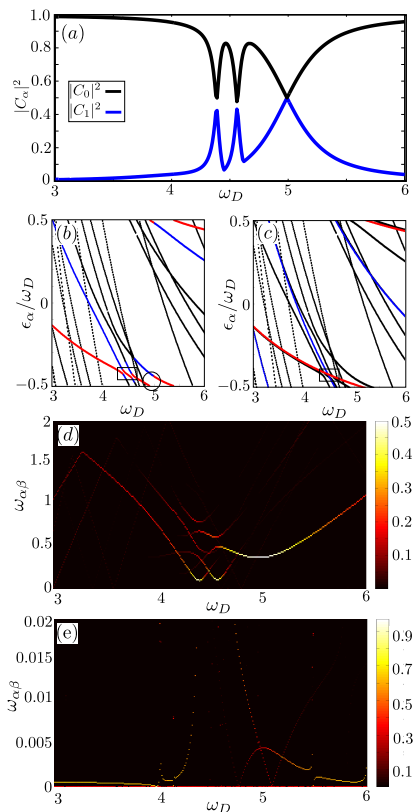


FIG. 3: On-site dynamics for a single particle. (a) Populations $|C_0|^2$ and $|C_1|^2$ of the two most populated FMs. (b) QE spectrum as a function of the driving frequency ω_D (measured in units of ω_R). Highlighted are the most (red) and second most (blue) populated FMs. The rectangular area indicates the narrow avoided crossings, while the circle highlights the area where a broad avoided crossing among the FMs appears with respect to the driving frequency. (c) In black is again the QE spectrum (same as in (b)). Additionally, we show the most (red) and second most (blue) populated states of the static, i.e. undriven, lattice. For comparison, we depict again the black rectangle at the same position as in (b). (d) Frequencies $\omega_{\alpha\beta}$ of the on-site dynamics as a function of the driving frequency (see main text). (e) Same as (d), but in the triple well setup (shown is only the extract of small frequencies $\omega_{\alpha\beta} \ll \omega_D$ which corresponds to tunneling dynamics). In all panels $A = 0.05$.

simplify the setup studied in Sec. III.A to just a single well of the lattice potential. Hence, the potential is given by $V_{sh}(x, t) = V_0 \sin^2(x - A \sin(\omega_D t))$ for $x \in (-\pi, +\pi]$ and we impose periodic boundary conditions at $x = \pm\pi$ in order to mimic the situation in an extended lattice. We choose as initial state $\Psi(x, 0)$ the single particle density as shown in Fig. 2(b) at $t = 0$ within the central potential well. The time evolution is then obtained by expanding $\Psi(x, 0)$ in terms of the FMs of the system and by making use of Eq. (6). As a result, we find that we can reproduce some of the main features of the on-site dynamics shown in Figs. 2(a) and (b), namely, we observe resonantly enhanced on-site oscillations in an interval of

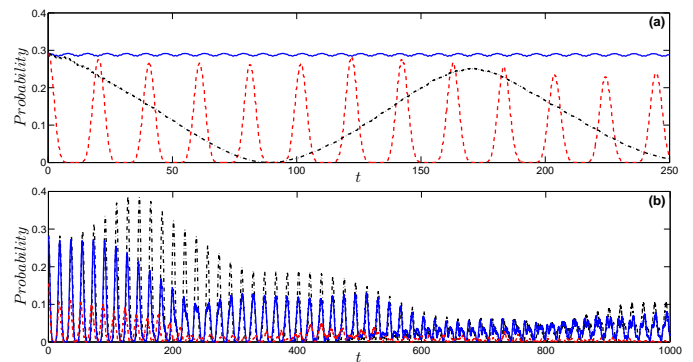


FIG. 4: (a) Tunneling probability (see main text) $|D_{\{N_i\};\mathbf{I}}|^2 = |\mathbf{I} \langle 2, 1, 1 | \Psi(t) \rangle|^2$ with $I_L = (2, 0, 0)$ and $I_R = I_M = (1, 0, 0)$ as a function of time for different driving frequencies $\omega_D = 0.5$ (blue solid line), $\omega_D = 4.5$ (red dashed line) and $\omega_D = 11.0$ (black dashed-dotted line). The most significant contribution of the interband tunneling mode is between the state $|2, 1, 1\rangle_{\mathbf{I}}$ [with $I_L = (2, 0, 0)$ and $I_R = I_M = (1, 0, 0)$] and the initial $|1, 2, 1\rangle_{\mathbf{I}}$ [with $I_M = (2, 0, 0)$ and $I_R = I_L = (1, 0, 0)$]. (b) Inter-well tunneling probability $|D_{\{N_i\};\mathbf{I}}|^2$ at resonance for different values of the interatomic interaction $g = 0.1$ (black dashed-dotted line), $g = 0.5$ (blue solid line) and $g = 2.0$ (red dashed line). In all panels $A = 0.05$. The time evolution is expressed in units of ω_R^{-1} .

the driving frequencies around $\omega_D \approx 4.5$. Following the discussion in ref. [42], further insight into this effect can be obtained by studying the population of the FMs by the initial state as a function of ω_D . We therefore sort the FMs Ψ_α according to their overlap with the initial state and label the mode with the largest overlap as Ψ_0 , the mode with the second largest overlap as Ψ_1 etc. In Fig. 3(a) the coefficients of the two most populated FMs, $|C_0|^2$ and $|C_1|^2$, are shown as a function of the driving frequency. Apparently, both at small frequencies ($\omega_D \lesssim 4$) and at large ones ($\omega_D \gtrsim 5.5$) only a single FM is notably populated, while $|C_0|^2$ and $|C_1|^2$ become comparable at distinct driving frequencies (e.g., at $\omega_D \approx 5$). According to our discussion above, in cases when $|C_0|^2$ is close to one, and thus only a single FM is populated, the stroboscopic time evolution, as given by Eq. (6), becomes, to a good approximation, time periodic with the period of the driving T_D . Note that this agrees with the observation of Fig. 2(a), that away from the resonance frequencies, the single particle density merely performs oscillations whose period matches T_D . This corresponds precisely to the previously described micro-motion arising from the explicit time dependence of the FM $\Psi_0(x, t)$.

On resonance, when $|C_0|^2 \approx |C_1|^2$, the evolution of $|\Psi(x, 0)|^2$ includes, besides the micro-motion, an interference term between Ψ_0 and Ψ_1 , whose period is dictated by the corresponding quasi energies and is given by: $T_{\text{osc}}/T_D = \hbar\omega_D/(\epsilon_1 - \epsilon_0)$. Indeed, we find that this term is responsible for the observed on-site mode with a period of ~ 14 lattice oscillations [compare Fig. 2(b)]. Up to now, however, it is not yet clear why Ψ_1 is res-

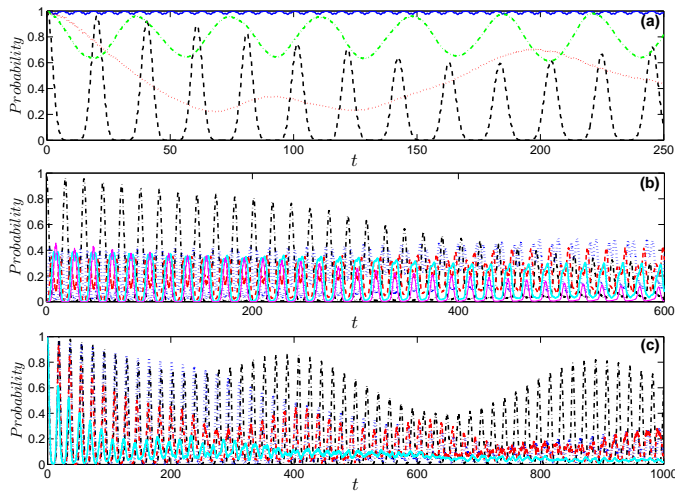


FIG. 5: (a) Probability $|B_{\{N_i\};\mathbf{I}}|^2$ (see main text) for all bosons to be in the zeroth-band during the evolution for different driving frequencies $\omega_D = 2.0$ (blue solid line), $\omega_D = 4.5$ (black dashed line), $\omega_D = 10.25$ (red dotted line) and $\omega_D = 11.75$ (green dashed-dotted line). (b) Comparison of different excitation scenarios at $\omega_D = 4.375$. The black dashed-dotted line refers to the probability for all the bosons to be in the zeroth-band while the blue dotted, red dashed, light-blue thick solid and magenta thin solid line refer to the probability to have one, two, three or four bosons, respectively, in the first-excited band. (c) Probability $|B_{\{N_i\};\mathbf{I}}|^2$ for all the bosons to be in the zeroth-band for $\omega_D = \omega_D^c$, but with different interparticle repulsion $g = 0$ (black dashed-dotted), $g = 0.1$ (blue dotted line), $g = 0.5$ (red dashed-dotted line) and $g = 2.0$ (light-blue solid line). In all panels $A = 0.05$. The time evolution is expressed in units of ω_R^{-1} .

onantly populated at certain frequencies. In order to provide an answer to this question we follow the argumentation in ref. [42] and consider the dependence of the quasi energy spectrum on the driving frequency ω_D as shown in Fig. 3(b). Highlighted are the two most populated modes at each ω_D (blue and red dots) revealing avoided crossings of these two modes at the frequencies where a resonant enhancement of $|C_1|^2$ was observed in Fig. 2(b). Hence, at these values of ω_D the FMs Ψ_0 and Ψ_1 are resonantly coupled by the driving which results in an increase of $|C_1|^2$ and ultimately to the in Sec. III.A described on-site dynamics.

In the following we provide insight into the question why we observe Floquet resonances at driving frequencies around $\omega_D \sim 4.5$. Let us start by noting that, by means of appropriate unitary transformations, the single particle Hamiltonian with a potential as given in Eq. (1) can be recasted into the form:

$$\tilde{H} = -\frac{\hbar^2}{2m} \frac{\partial^2}{\partial x^2} + V_0 \sin^2(k_0 x) + V_D \sin(\omega_D t)x, \quad (7)$$

where the amplitude of the oscillating term is given by $V_D = mA\omega_D^2$. That is the transformed Hamiltonian takes the form of a static lattice plus a time-dependent perturbation whose strength is determined by V_D . For the

used parameters of $m = 1$ and $A = 0.05$ and for the range of considered frequencies of $3 \lesssim \omega_D \lesssim 6$ we get that the amplitude V_D of the time-dependent term is of order one. Hence, it can be seen as a small perturbation compared to the static term of strength $V_0 = 15$ and we can expect that the QEs of the driven lattice setup can be estimated by the actual energies of the undriven lattice. Resonances would then be expected whenever the energy difference between two notably populated eigenstates of the static system matches an integer multiple of $\hbar\omega_D$. In fact we find that the energies of the three energetically lowest states of even parity are given by $E_0 \approx 2.6$, $E_1 \approx 11.6$ and $E_2 = 16.9$. Naively, we expect driving induced resonances whenever the ground state is resonantly coupled to one of the excited states. Indeed we find $E_1 - E_0 \approx 2 \times 4.5$ and $E_2 - E_0 \approx 3 \times 4.8$. Thus, following this line of arguments, at driving frequencies of approximately $\omega_D = 4.5$ the ground state of the unperturbed lattice is coupled via a 2 (3) photon process to the first (second) excited states. In order to justify this simplified picture we show the energies E_0 and E_1 on top of the QE spectrum of the driven lattice (see Fig. 3(c)). Away from any resonances, both energies are almost identical to the QEs of the corresponding Floquet states, so e.g. the red line is practically on top of an underlying black line. Closer to the resonance region, we see of course deviations of the QEs from the mere energies of the undriven lattice as the different states are coupled by the driving.

Finally, Fig. 3(c) provides an overview over the possibly observed frequencies in the on-site dynamics at various driving frequencies. Shown are the frequencies associated to all possible interference terms between the FMs weighted by their overlap with the initial state. More precisely, we calculate $\omega_{\alpha\beta} = (\epsilon_\alpha - \epsilon_\beta)/\hbar$ for all pairs of FMs at a given driving frequency and determine the colour coding by computing the product $|C_\alpha^* C_\beta|$. Hence, the frequency $\omega_{\alpha\beta}$ appears in Fig. 3(c) only when both of the corresponding FMs Ψ_α and Ψ_β have appreciable overlap with the initial state. In agreement with the discussion concerning Fig. 3(b) we observe pronounced on-site oscillations only within an interval of driving frequencies $4.0 \lesssim \omega_D \lesssim 5.5$. In particular, the two narrow avoided crossings around $\omega_D^c \approx 4.5$ [see the rectangular in Fig. 3(b)] yield a low frequency on-site dynamics, whereas the comparably broad avoided crossing at $\omega_D \approx 5$ [see the circle in Fig. 3(b)] results in a much faster on-site oscillation.

3. Tunneling dynamics in the triple well

Besides the on-site dynamics, Fig. 2(b) revealed a pronounced tunneling between the lattice sites at certain driving frequencies. Similar to the previous section, we analyze this effect in the following by applying Floquet theory for the single particle dynamics. We choose the same setup as before, that is, $V_{sh}(x, t) =$

$V_0 \sin^2(x - A \sin(\omega_D t))$, with the same initial state, i.e. essentially a Gaussian centered around the potential well at $x = 0$, but with the difference that the periodic boundary conditions are imposed at $x = \pm 2\pi$ (instead of at $x = \pm \pi$ as we did before). In this way we allow for tunneling of the wave packet into the two neighbouring lattice sites. As for the on-site dynamics, we provide an overview over the observable frequencies in the temporal evolution in Fig. 3(d) [in close analogy to Fig. 3(c)]. Note that, since the tunneling dynamics observed in Sec. III.A occurs on much longer timescales as compared to the on-site dynamics, we only show the extract of the regime of small frequencies, i.e. $\omega_{\alpha\beta} \ll \omega_D$. Furthermore, because no on-site dynamics occurs with timescales matching the extremely small frequencies of $\lesssim 0.02$, all the frequencies depicted in Fig. 3(d) are indeed associated with an inter-well tunneling mode. In accordance with the observation made in the many-particle simulations [cf. Fig. 2(b)] we observe a strong increase of the frequencies associated with the tunneling dynamics in the range of driving frequencies of $4 \lesssim \omega_D \lesssim 5.5$. Away from this resonance, for example at $\omega_D = 2.5$, the only notable tunneling mode corresponds to an interference term of two FMs which oscillates with a period of $T_{\text{osc}}/T_D \approx 3300$ and could therefore not be observed in the simulations performed in Sec. III.A. Within the regime of resonant driving, e.g. at $\omega_D = 4.5$, the frequency of the tunneling mode is increased strongly and the associated oscillation period becomes $T_{\text{osc}}/T_D \approx 200$ matching the observed tunneling mode in the weakly interacting regime [cf. Fig. 2(b)].

C. Interband tunneling and excitation processes

In the previous section we have shown that most of the features of the (effective) single-particle dynamics of Fig. 2 can be explained via a non-interacting Floquet theory. As we shall see now, however, the full dynamics presents a rich excitation spectrum ascribable to the particles interaction, especially in the strong interaction regime. Thus, we investigate the tunneling and excitation probabilities of the dominant particle configurations, for different driving frequencies ω_D , by means of the multiband expansion introduced in Sec. II.C. More precisely, we compute and analyze the probabilities, during the dynamics, defined as

$$|C_{\{N_i\};\mathbf{I}}|^2 = |\mathbf{I} \langle N_1, N_2, N_3 | \Psi(t) \rangle|^2. \quad (8)$$

The case $I_m^{(k)} = 0 \forall k > 1$ refers to the lowest-band inter-well tunneling dynamics. The initial state of the system corresponds to the ground state of four weakly interacting bosons with $g = 0.1$ in a triple well, while the dominant number state configuration (see also Sec.II.C) is $|1, 2, 1\rangle_{\mathbf{I}}$ with $I_L = I_R = (1, 0, 0)$ and $I_M = (2, 0, 0)$. In this way, a lowest-band tunneling process can take place among the initial state and: a) another state of single-pair occupancy, e.g. $|2, 1, 1\rangle_{\mathbf{I}}$ ($I_L = (2, 0, 0)$ and

$I_M = I_R = (1, 0, 0)$), b) a state with double-pair occupancy, e.g. $|2, 2, 0\rangle_{\mathbf{I}}$ ($I_L = I_M = (2, 0, 0)$ and $I_R = (0, 0, 0)$), c) a state with triple occupancy, e.g. $|3, 1, 0\rangle_{\mathbf{I}}$ ($I_L = (3, 0, 0)$, $I_M = (1, 0, 0)$, $I_R = (0, 0, 0)$) or d) a state with quartic occupancy, e.g. $|4, 0, 0\rangle_{\mathbf{I}}$ ($I_L = (4, 0, 0)$ and $I_M = I_R = (0, 0, 0)$). However, the from the system preferred tunneling processes form a hierarchy according to the energetical difference between the initial and final state. For instance, a tunneling process to another state of single-pair occupancy will be more preferable than to a state of double-pair occupancy etc. Figure 4(a) shows the tunneling probability to the energetically closest number state, which is $|2, 1, 1\rangle_{\mathbf{I}}$ (or $|1, 1, 2\rangle_{\mathbf{I}}$) with $I_L = (2, 0, 0)$ and $I_M = I_R = (1, 0, 0)$ (or $I_L = I_M = (1, 0, 0)$ and $I_R = (2, 0, 0)$), i.e. $|D_{\{N_i\};\mathbf{I}}|^2 = |\mathbf{I} \langle 2, 1, 1 | \Psi(t) \rangle|^2$ with $I_L = (2, 0, 0)$ and $I_M = I_R = (1, 0, 0)$, for various driving frequencies. As it is shown, for $\omega_D < \omega_D^c$ this tunneling mode has a small amplitude and it is quite insensitive to ω_D as intuitively expected from the fact that the evolved-state is essentially unperturbed by the driving (see also Fig. 1(a)). For $\omega_D \approx \omega_D^c$, however, the amplitude of the oscillations is significantly larger indicating an enhancement of the tunneling (see also Figs. 2(b) and 3(d)), whereas when $F_{\omega_D} \ll 1$ and $\omega_D > \omega_D^c$ ($\omega_D = 11.0$ curve in Fig. 4(a)) the oscillations occur with a larger period. The fact that it oscillates with a larger time period can be traced back to the behaviour of the fidelity at $\omega_D = 11$. Indeed, for short times ($\omega_D = 11.0$) the system stays in the initial ground state and after some time the fidelity starts to decrease, differently from the situation at $\omega_D = 4.5$, where the system deviates from the initial state on much shorter time scales. Concerning the remaining tunneling modes, i.e. tunneling to higher energetical states that belong to the lowest-band (see discussion above), they are negligible as they provide a very small contribution even for $\omega_D = \omega_D^c$. The latter has already been seen in the last subsection, but it can also be shown with the use of the multi-band analysis. On the other hand, Fig. 4(b) presents again the tunneling probability $|D_{\{N_i\};\mathbf{I}}|^2$ for the energetically closest lowest-band states (i.e. same as Fig. 4(a)) when the driving frequency is at resonance for different interaction strengths g . For weak to intermediate interactions the tunneling amplitude decreases and for strong interactions, e.g. $g = 2.0$, a destruction of the tunneling is observed for long time scales.

Now, let us consider the excitation dynamics. In this case it holds $I_m^{(k)} \neq 0$ for $k > 1$. To this aim, we have analyzed the probability of finding all the four bosons in the zeroth-band. The latter, can be expressed via eq.(7) as $|B_{\{N_i\};\mathbf{I}}|^2 = \sum_{\mathbf{I}} |\mathbf{I} \langle N_1, N_2, N_3 | \Psi(t) \rangle|^2 = \sum_{\mathbf{I}} |C_{\{N_i\};\mathbf{I}}|^2$, where the summation is performed over the excitation indices $\mathbf{I} = (I_L, I_M, I_R)$ which, in terms of the multiband expansion, obey the constraints $I_L^{(1)} + I_M^{(1)} + I_R^{(1)} = N$ and $I_L^{(j)} = I_M^{(j)} = I_R^{(j)} = 0$ for all $j > 1$. In particular, Fig. 5(a) shows the probability $|B_{\{N_i\};\mathbf{I}}|^2$ for all the bosons to reside in the zeroth-band for various driving frequen-

cies ω_D and a fixed amplitude $A = 0.05$ during the time evolution. At the critical driving frequency a complete depopulation of the zeroth-band at some specific time intervals is observed. In particular, this probability exhibits revivals, which are connected with the enhancement of the (amplitude) oscillations of the single-particle density [see also Fig. 2(b)]. On the other hand, for driving frequencies different from the critical frequency the respective probability for all the bosons to occupy the zeroth-band is rather large and is indeed dominant. However contributions from excited configurations cannot be neglected, especially in the regions $7.0 < \omega_D < 8.0$ and $10.0 < \omega_D < 15.0$, where the system significantly departs from the initial state [see also Fig. 1(a) and Fig. 5(a) red dashed line]. Furthermore, Fig. 5(b) presents the probability, at the critical driving frequency, to obtain a state of $N_0 \leq 4$ particles in the first-excited band and the remaining to be in the zeroth-band. The latter can be expressed as $|Q_{\{N_i\};\mathbf{I}}|^2 = \sum_{\mathbf{I}} |C_{\{N_i\};\mathbf{I}}|^2$ where the summation index $\mathbf{I} = (I_L, I_M, I_R)$ obeys the constraints $I_L^{(1)} + I_M^{(1)} + I_R^{(1)} = N - N_0$, $I_L^{(2)} = I_M^{(2)} = I_R^{(2)} = N_0$ and $I_L^{(j)} + I_M^{(j)} + I_R^{(j)} = 0$ for all $j > 2$. Indeed, the interplay between the four possible excitation scenarios from the zeroth to the first excited-band (i.e. one-particle excitation, two-particle excitation etc) in the course of the dynamics is illustrated in a transparent way. It is observed that the complete depopulation of the zeroth-band is mainly accompanied by the excitation of three or all the four bosons in the first-excited band. For long evolution times the zeroth-band possesses a low population and states with one or two bosons in the first excited-band are mainly populated. The states with the most significant contribution are of the type $|1, 2, 1\rangle_{\mathbf{I}}$ with $I_L = I_R = (0, 1, 0)$ and $I_M = (0, 2, 0)$ or $I_M = (1, 1, 0)$. We note that a small contribution comes from the state $|1, 2, 1\rangle_{\mathbf{I}}$ with $I_L = I_R = (0, 1, 0)$ and $I_M = (0, 1, 1)$. This clearly shows that the most prominent excitation process in our system originates from the energy difference between each of the above states and $|1, 2, 1\rangle_{\mathbf{I}}$ with $I_L = I_R = (1, 0, 0)$ and $I_M = (2, 0, 0)$, namely the (initial) ground state configuration.

Finally, in order to explore the impact of the interactions on the dynamics, Fig. 5(c) shows the probability $|B_{\{N_i\};\mathbf{I}}|^2$ for long evolution times for all the bosons to be in the zeroth-band for different interparticle repulsion at the driving frequency $\omega_D = \omega_D^c$. For the non-interacting case the population of the zeroth-band shows revivals even for long time scales, while, as the interaction strength is turned on, the corresponding probability presents a decaying envelope. This envelope behaviour is a pure effect of the interactions and reflects also the initial ground state configuration (see the discussion in Sec. II.C) which strongly depends on the interparticle interactions. As it can be seen for increasing repulsion between the particles the probability for the system to remain in the zeroth-band, in the course of the dynamics, decays on increasingly shorter time scales and the system is dominated by different types of excitations, as

expected intuitively.

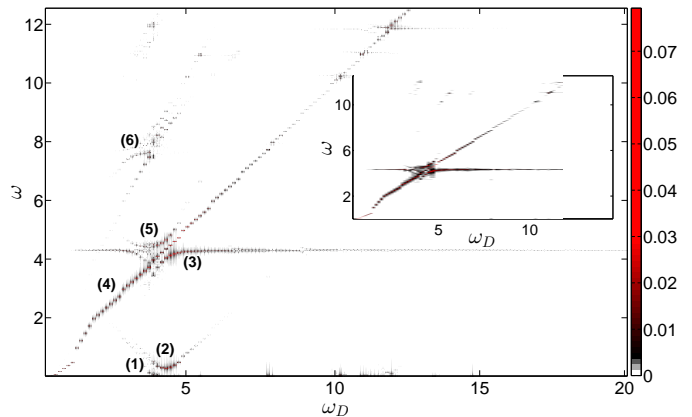


FIG. 6: Local one-body density spectrum $\rho_L(\omega)$ (for the left well) as a function of the driving frequency ω_D (measured in units of ω_R). The driving amplitude has been chosen $A = 0.05$. Inset: the spectrum of the intra-well oscillations calculated via $\Delta\rho_L(t)$ (see also main text).

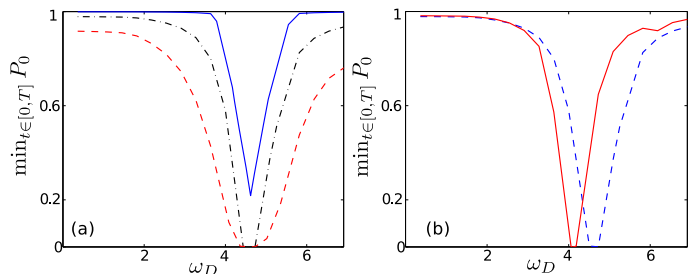


FIG. 7: (a) Profile of the resonance for various driving amplitudes $A = 0.01$ (blue solid line), $A = 0.05$ (black dashed-dotted line) and $A = 0.1$ (red dashed line) obtained from the $\min_{t \in [0, T]} P_0(t)$ and T being some fixed long evolution time, as a function of the driving frequency. (b) Same as (a) with $A = 0.05$, but for different barrier heights $V_0 = 9.0$ (red solid line) and $V_0 = 12.0$ (blue dashed line). The system consists of four bosons confined in a triple-well with interparticle interaction $g = 0.1$.

D. Characteristics of the resonant behaviour

To characterize the overall process with respect to the driving frequency, we compute the spectrum of the local one-body density

$$\rho_\alpha(\omega) = \frac{1}{\pi} \int_0^T dt \rho_\alpha(t) e^{i\omega t}, \quad (9)$$

where $\rho_\alpha(t) = \int_{d_\alpha} dx \rho_1(x, t)$ denotes the spatially over a single well integrated single-particle density at every time instant t . The index $\alpha = L, M, R$ corresponds to the left, middle or right well respectively, whereas the limits of

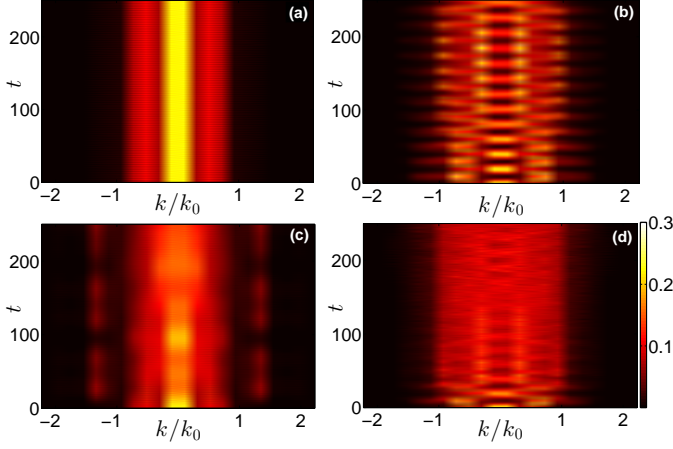


FIG. 8: Momentum distribution of the one-body density as a function of time (measured in units of ω_R^{-1}) for $g = 0.1$ and different driving frequencies (a) before the critical frequency $\omega_D = 2.0$, (b) at the critical frequency $\omega_D = \omega_D^c = 4.5$ and (c) at $\omega_D = 8.0$. (d) The case of strong interparticle repulsion for $g = 2.0$ and $\omega_D = \omega_D^c$. The horizontal axis represents the lattice momenta in units of the inverse lattice vector $k_0 = \pi/l$. In all panels $A = 0.05$.

the wells are denoted by d_α, d'_α . Note that in the present case all the components of $\rho_\alpha(\omega)$, i.e. $\rho_L(\omega)$, $\rho_M(\omega)$ and $\rho_R(\omega)$, are equivalent due to the considered large lattice depths and the employed driving scheme which enforces the bosons among different wells to oscillate in-phase. Figure 6 shows the above spectrum, where five dominant branches (denoted as (1) to (5) in the Figure) can be observed. The lowest branch denoted as (1) in Fig.6 (in the range $\omega \in [0, 0.02]$) refers to the intraband tunneling being restricted to the energetically closest number states e.g. from $|1, 2, 1\rangle_{\mathbf{I}}$ ($I_M = (2, 0, 0)$, $I_L = I_R = (1, 0, 0)$) to $|2, 1, 1\rangle_{\mathbf{I}}$ ($I_L = (2, 0, 0)$, $I_M = I_R = (1, 0, 0)$). This branch is hardly visible in Fig.6 due to the presented wide range of frequencies that have been taken into account in order to visualize all the dynamical frequencies of the system. In addition, the next lowest branch (denoted as (2)) at $\omega_D \in [4, 5]$ and $\omega \in [0.05, 1]$ corresponds to the large amplitude density oscillations [see also Fig. 2(b)]. These mode frequencies have been already predicted via the Floquet analysis in Sec. III.B [see Fig. 3(c) and (d)]. To investigate in some detail the intra-well wavepacket dynamics the quantity $\Delta\rho_\alpha(t) = \rho_{\alpha,1}(t) - \rho_{\alpha,2}(t)$ is employed. Here, each well is divided from the center into two equal parts, namely left and right, with $\rho_{\alpha,1}(t)$, $\rho_{\alpha,2}(t)$ being the corresponding integrated densities at time t . The index $\alpha = L, M, R$ stands for the left, middle and right well, respectively. To determine the frequencies of this mode we calculate the spectrum $\Delta\rho_L(\omega) = \frac{1}{\pi} \int dt \Delta\rho_L(t) e^{i\omega t}$. The inset of Fig. 6 presents the corresponding spectrum, thus showing the emergent frequencies of the intra-well oscillations as a function of the driving frequency ω_D . We observe that the spectrum $\Delta\rho_L(\omega)$ follows the evolution of the upper three branches

(denoted by (3), (4) and (5)) of the spectrum of $\rho_L(\omega)$, whereas in the region of the resonance the intra-well oscillation measured via $\Delta\rho_L(t)$ features a beating dynamics, as expected. Hence, away from the region around the critical driving frequency the generated dipole mode possesses three different frequencies, while close to ω_D^c the intra-well dynamics come into a resonance. Therefore, one can induce this resonant intra-well dynamics by adjusting the driving frequency. Finally, let us comment on the existence of some higher frequency components, e.g. branch (6) in Figure 6, which correspond to very fast intrawell oscillations (i.e. $\omega \ll \omega_D$) and possess a low amplitude (in comparison to the previous branches (1)-(5)).

In turn, we shall visualize the above mentioned resonance and inspect how it depends on the lattice parameters. To this aim, the minimal occupancy, during the evolution time T , of the zeroth-band $\min_{t \in [0, T]} P_0(t) = \min_{t \in [0, T]} \sum_{\mathbf{I}} |\langle N_1, N_2, N_3 | \Psi(t) \rangle|^2$, with the energetical indices $I_L^{(1)} + I_M^{(1)} + I_R^{(1)} = N$ and $I_L^{(j)} = I_M^{(j)} = I_R^{(j)} = 0$ for every $j > 1$ is used. Employing the above quantity one can show that far from resonance there are regions with non-negligible excitations i.e. $\min_{t \in [0, T]} P_0 < 1$ [e.g. at $\omega_D = 11.0$ see also Fig. 1(a)] as well as regions where $\min_{t \in [0, T]} P_0 \approx 1$ [e.g. $\omega_D = 2.0$ in Fig. 1(a)]. Now let us analyze the dependence of $\min_{t \in [0, T]} P_0$ on the driving frequency around ω_D^c . Firstly we study the dependence of the resonance on the driving amplitude. In Figure 7(a) we show for an increasing driving amplitude the minimum of $\min_{t \in [0, T]} P_0$ as a function of the frequency ω_D which broadens and eventually reaches zero, meaning that the zeroth-band has been complete depopulated [see also Fig. 5(a)]. On the other hand, for small amplitudes the value of the minimum of $\min_{t \in [0, T]} P_0$ is non-zero and in the limit $A \rightarrow 0$ its dependence on the driving frequency disappears. Instead, in Fig. 7(b) we show how the minimal population of the zeroth-band ($\min_{t \in [0, T]} P_0$) varies as a function of the lattice depth. For an increasing lattice depth it is known that the energy gaps among the different energy levels become larger. This phenomenon can intuitively be understood in terms of a tight-binding approximation. For simplicity let us assume only a nearest neighbour coupling $J \propto \int dx W_s(x) [\frac{p^2}{2m} + V_0 \sin^2(x)] W_{s+1}(x)$ between the sites s and $s+1$, where $W_s(x)$ are the on-site localized Wannier states. Then, within this approximation, which is valid for a relatively deep potential, the resulting eigenvalues are $E_{k-1} = E_0^{on-site} - 2J \cos(\frac{k\pi}{N+1})$ ($k = 1, 2, \dots, N$), where $E_0^{on-site}$ are the on-site energies. Thus, the resonance can be tuned at will, i.e. for a decreasing lattice depth the ω_D^c is negatively shifted, as it is confirmed by the numerical results of Fig. 7(b). Finally, let us comment on the dependence of the position of the resonance on the interparticle interaction strength g . Indeed, in order to investigate whether there is such a dependence various interaction strengths (for the same particle number $N = 4$), e.g. $g = 0.1$, $g = 1.0$ and

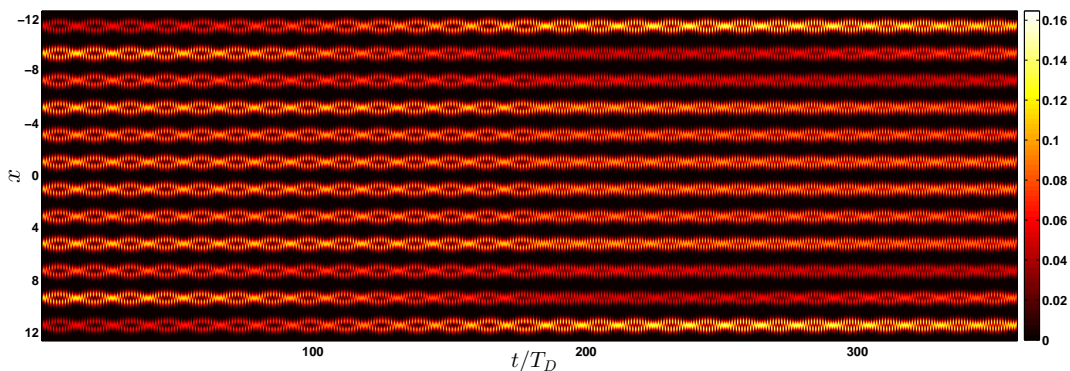


FIG. 9: Time evolution of the one-body density $\rho_1(x, t)$ in a twelve-well potential for $\omega_D = 4.5$. The driving amplitude is fixed to the value $A = 0.05$, while the initial state corresponds to the ground state of five weakly interacting bosons with $g = 0.1$. The spatial extent of the lattice is expressed in units of k_0^{-1} , while the time units are rescaled in terms of the driving period T_D .

$g = 3.0$, have been considered (omitted here for brevity) and it was found that the position of the resonance is essentially unaffected.

In the following, let us inspect the momentum distribution with varying driving frequency with the aim of understanding whether signatures of a parametric amplification of matter-waves can be observed. The momentum distribution is a routinely employed observable in atomic quantum gases experiments as it is accessible via time-of-flight measurements [4]. This quantity can be calculated as the Fourier transformation of the one-body reduced density matrix as

$$n(k, t) = \frac{1}{2\pi} \iint dx dx' \rho_1(x, x'; t) e^{-ik(x-x')}. \quad (10)$$

Here $\rho_1(x, x'; t)$ denotes the one-body reduced density matrix, being obtained by tracing out all the bosons but one in the density of the N -body system. The panels 8(a)-(c) of Fig. 8 present the time evolution of the momentum distribution for different driving frequencies before, on, and after the resonance. As it can be noted, exactly at the resonance the momentum distribution exhibits a special pattern, that is, some additional lattice momenta are periodically activated during the dynamics. In particular, it is observed that the modes $\pm \frac{k_0}{2} \simeq \pm 1.57$, $\pm k_0 \simeq \pm 3.14$, $\pm \frac{3k_0}{2} \simeq \pm 4.713$ are populated, whereas out of resonance only the $\pm k_0$ modes are significantly populated. The population of the $\pm k_0/2$, $\pm 3k_0/2$ modes at $\omega_D = \omega_D^c$ is reminiscent of the parametric amplification of matter-wave phenomenon, as observed experimentally in ref. [21]. However, an exact correspondence with ref. [21] cannot be made due to the very different setup of our system, i.e. its finite size and the hard wall boundaries. A detailed study of this process, also for higher particle numbers and lattice potentials, would be desirable, but it is clearly beyond the scope of this work. Furthermore, Fig. 8(d) shows the momentum distribution at resonance, but for a strong interparticle repulsion $g = 2.0$. The expected periodic pattern for large evolution times

is blurred as an effect of the strong interaction which decreases the degree of coherence.

Finally, in order to demonstrate that our findings are of general character we investigate a larger lattice system with a filling factor smaller than unity. Specifically, the case of five bosons in a twelve-well finite lattice has been considered. Concerning the ground state with filling factor $\nu < 1$, the most important aspect is the spatial redistribution of the atoms as the interaction strength increases. Indeed, as the repulsion increases from the non-interacting to the weak interaction regime the atoms are pushed from the central to the outer sites which gain and lose population in the course of increasing g .

In the following, the shaking dynamics applied at $t = 0$ to the ground state of the five bosons which are trapped in the twelve-well potential in the weak interaction regime ($g = 0.1$) is explored. The emergent non-equilibrium behaviour shows similar characteristics as in the previous setup with filling $\nu > 1$, i.e. the occurrence of an intrawell dipole and an interwell tunneling mode. Interestingly, at the same frequency $\omega_D = \omega_D^c = 4.5$ a resonance of the intra-well dynamics is observed. Figure 9 presents the one-body density evolution exactly at the critical point ω_D . As in the case for setups with filling $\nu > 1$, the formation of enhanced density oscillations at each site is observed, which is in relation to the time periods where the zeroth-band is completely depopulated during the evolution. Employing a corresponding number state analysis the significant contribution of two kinds of number states has been confirmed: a) Either $I_1^{(1)} + \dots + I_{12}^{(1)} = N - 1$, $I_1^{(3)} = \dots = I_{12}^{(3)} = 0$ and one with $I_k^{(2)} = 1$ for $k = 1, \dots, 12$ or b) $I_1^{(1)} + \dots + I_{12}^{(1)} = N - 1$, $I_1^{(2)} = \dots = I_{12}^{(2)} = 0$ and a certain $I_k^{(3)} = 1$ for $k = 1, \dots, 12$. Notice that the same kind of number states have been found to contribute significantly also in the dynamics of four bosons in the triple-well. The above mentioned observations suggest a generalization of the observed phenomena to larger systems as well. Indeed,

the same shaken scheme has been tested in different systems (omitted here for brevity), e.g. 10 bosons in a triple-well, 6 bosons in five wells etc, confirming that the above observed resonant-like behaviour of the bosonic ensemble occurs in each setup.

IV. Conclusions and Outlook

The correlated non-equilibrium quantum dynamics of few-body bosonic ensembles induced by the driving of a finite-size optical lattice has been investigated. Our work focuses particularly on the regimes of large lattice depths and small driving amplitudes. This choice has been made in order to limit the degree of excitations that would otherwise lead to heating processes. Starting from the ground state of a weak or strongly interacting small ensemble, we have examined in detail the time evolution of the system induced by periodically driving the optical lattice. We find that the dynamical evolution of the system is governed by two main modes: the inter-well tunneling and the intra-well dipole-like mode. The dynamical behaviour of the system in the non-interacting regime has been firstly analyzed via Floquet theory, that is, at the single-particle level, providing an accurate interpretation of the observed processes. For large particle numbers and large interaction strengths, however, such a single-particle description was not anymore sufficient to provide an exhaustive explanation of the observed dynamics, and a multi-band Wannier number state expansion has been employed.

The inter-well tunneling mode is weak as a consequence of the deep optical lattice and the small driving amplitude. On the other hand, the local dipole mode has been identified from the intra-well oscillations of bosons in the individual wells. Remarkably enough, it has been found that by tuning the driving frequency the intra-well dynamics experiences a resonant-like behaviour. This is manifested e.g. by the enhanced oscillations in the one-body density evolution or from the periodic population of additional lattice momenta in the momentum distribution of the one-body density. Additionally, on a single-particle level in terms of Floquet theory, it has been shown that in the proximity of the resonance the first two FMs possess the main contribution, while away from resonance the dynamics can be described with the inclusion of the first FM. To explain the enhanced population of the second FM at resonance the corresponding quasienergy spectrum has been employed, revealing avoided-crossings between the first two FMs at certain driving frequencies. To obtain the frequencies which refer to the on-site and tunneling dynamics, the corresponding frequencies associated with the interference terms between the FMs have been employed showing pronounced on-site oscillations and an enhancement of the inter-well tunneling mode in the vicinity of the resonance. Considering an ensemble of few-bosons we examined the influence of the interatomic interactions both for the inter-

and intra-well generated modes. Indeed, it has been found that the repulsion affects each of the aforementioned modes, yielding a destruction of the inter-well tunneling for strong interactions and an enhancement of the excitations (i.e. the contribution of higher-band states). Moreover, in the spectrum of the local one-body density with respect to the driving frequency all the relative dynamical frequencies, e.g. on-site oscillations and tunneling period have been identified. Finally, the occurrence of the above resonance seems to be universal in a periodically driven lattice as it is independent of the filling factor, the boundary conditions or the interparticle repulsion.

We would like to underline that, contrarily to related studies based e.g. on effective model Hamiltonians or lattice calculations with tensor network methods, our many-body analysis based on the ab initio MCTDHB method has the advantage to provide the complete system wavefunction in space and time. Thus, it enables us to accurately identify the involved intra- and inter-well band excitations.

Let us comment on possible future investigations. Although in the present work we did not employ the multi-layer structure of the ML-MCTDHB method, our ab-initio approach is well suited to describe the dynamics of multi bosonic species. Given this, a first natural extension would be to study the driven dynamics of mixtures consisting of different bosonic species in order to unravel the induced excitation modes or to devise schemes for selective transport of an individual bosonic component. In relation to the present study, it would be interesting to simulate the parametrical amplification of matter-waves with interesting applications, like the generation of four-wave mixing, entanglement production, but also for fundamental tests of quantum mechanics with massive particles like the Hong-Ou-Mandel experiment, as recently performed with a Bose-Einstein condensate [23].

A. Appendix A: The Computational Method: ML-MCTDHB and MCTDHB

Our computational approach to solve the many-body Schrödinger equation of the interacting bosons relies on the Multi-Layer MultiConfiguration Time-Dependent Hartree method for Bosons (ML-MCTDHB) [43, 44] which constitutes an ab-initio method for the calculation of stationary properties and in particular the non-equilibrium quantum dynamics of bosonic systems of different species. For a single species it reduces to MCTDHB which has been established in refs. [32, 33, 45] and applied extensively [45–48]. The wavefunction is represented by a set of variationally optimized time-dependent orbitals which implies an optimal truncation of the Hilbert space by employing a time-dependent moving basis where the system can be instantaneously optimally represented by the corresponding time-dependent permanents. To be self contained let us briefly introduce

the basic concepts of the method and discuss the main ingredients of our implementation.

Within the MCTDHB method the time-dependent Schrödinger equation $(i\hbar\partial_t - H)\Psi(x,t) = 0$ is solved as an initial value problem $|\Psi(0)\rangle = |\Psi_0\rangle$. The many-body wavefunction which is expanded in terms of the bosonic number states $|n_1, n_2, \dots, n_M; t\rangle$, based on time-dependent single-particle functions (SPFs) $|\phi_i(t)\rangle$, $i = 1, 2, \dots, M$, reads

$$|\Psi(t)\rangle = \sum_{\vec{n}} C_{\vec{n}}(t) |n_1, n_2, \dots, n_M; t\rangle. \quad (\text{A1})$$

Here M is the number of SPFs and the summation \vec{n} is over all the possible particle combinations n_i such that the total number of bosons is conserved and equal to N . To determine the time-dependent wave function $|\Psi(t)\rangle$ we need the equations of motion for the coefficients $C_{\vec{n}}(t)$ and of the SPFs $|\phi_i(t)\rangle$. Following the Dirac-Frenkel [49, 50] variational principle i.e. $\langle \delta\Psi | i\partial_t - \hat{H} | \Psi \rangle = 0$ we end up with the well-known MCTDHB equations of motion [32, 33, 45, 51] consisting of a set of M non-linear integrodifferential equations of motion for the orbitals which are coupled to the $\frac{(N+M-1)!}{N!(M-1)!}$ linear equations of motion for the coefficients.

For our numerical implementation a discrete variable representation (DVR) for the SPFs and a sin-DVR, which intrinsically introduces hard-wall boundaries at both edges of the potential, has been employed. The

preparation of the initial state has been performed by using the so-called relaxation method in terms of which one obtains the lowest eigenstates of the corresponding m -well setup. The key idea is to propagate some trial wave function $\Psi^{(0)}(x)$ by the non-unitary operator $e^{-H\tau}$. This is equivalent to an imaginary time propagation and for $\tau \rightarrow \infty$, the propagation converges to the ground state, as all other contributions (i.e., $e^{-E_n\tau}$) are exponentially suppressed. In turn, we periodically drive the optical lattice and study the evolution of $\Psi(x_1, x_2, \dots, x_N; t)$ in the m -well potential within MCTDHB. To ensure the convergence of our simulations we have used up to 9 single particle functions thereby observing a systematic convergence of our results for sufficiently large spatial grids. An additional criterion that confirms the achieved convergence is the population of the lowest occupied natural orbital kept in each case below 0.1%.

Acknowledgments

S.M. thanks the Hamburgisches Gesetz zur Förderung des wissenschaftlichen und künstlerischen Nachwuchses (HmbNFG) for a PhD Scholarship. P.S gratefully acknowledges funding by the Deutsche Forschungsgemeinschaft (DFG) in the framework of the SFB 925 "Light induced dynamics and control of correlated quantum systems". A.N. gratefully acknowledges discussions with Klaus Mølmer related to four-wave mixing.

-
- [1] N. Goldman, and J. Dalibard, Phys. Rev. X **4**, 031027 (2014).
 - [2] N. Goldman, J. Dalibard, M. Aidelsburger, and N. R. Cooper, Phys. Rev. A **91**, 033632 (2015).
 - [3] O. Morsch, and M. Oberthaler, Rev. Mod. Phys. **78**, 179 (2006).
 - [4] I. Bloch, J. Dalibard, and W. Zwerger, Rev. Mod. Phys. **80**, 885 (2008).
 - [5] M. Olshanii, Phys. Rev. Lett. **81**, 938 (1998).
 - [6] R. Grimm, M. Weidemüller, and Y. B. Ovchinnikov, Adv. At. Mol. Opt. Phys. **42**, 95-170 (2000).
 - [7] L. Santos, M. A. Baranov, J. I. Cirac, H. U. Everts, H. Fehrmann, and M. Lewenstein, Phys. Rev. Lett. **93**, 030601 (2004).
 - [8] S. Inouye, J. Goldwin, M. L. Olsen, C. Ticknor, J. L. Bohn, and D. S. Jin, Phys. Rev. Lett. **93**, 183201 (2004).
 - [9] T. Köhler, K. Goral, and P. S. Julienne, Rev. Mod. Phys. **78**, 1311 (2006).
 - [10] C. Chin, R. Grimm, P. Julienne, and E. Tiesinga, Rev. Mod. Phys. **82**, 1225 (2010).
 - [11] M. Lewenstein, A. Sanpera, and V. Ahufinger, Ultracold Atoms in Optical Lattices: Simulating quantum many-body systems, (Oxford University Press, 2012).
 - [12] D. I. Choi, and Q. Niu, Phys. Rev. Lett. **82**, 2022 (1999).
 - [13] M. B. Dahan, E. Peik, J. Reichel, Y. Castin, and C. Salomon, Phys. Rev. Lett. **76**, 4508 (1996).
 - [14] O. Morsch, J. H. Müller, M. Cristiani, D. Ciampini, and E. Arimondo, Phys. Rev. Lett. **87**, 140402 (2001).
 - [15] E. Peik, M. B. Dahan, I. Bouchoule, Y. Castin, and C. Salomon, Phys. Rev. A **55**, 2989 (1997).
 - [16] M. Cristiani, O. Morsch, J. H. Müller, D. Ciampini, and E. Arimondo, Phys. Rev. A **65**, 063612 (2002).
 - [17] S. R. Wilkinson, C. F. Bharucha, K. W. Madison, Q. Niu, and M. G. Raizen, Phys. Rev. Lett. **76**, 4512 (1996).
 - [18] Q. Niu, X. G. Zhao, G. A. Georgakis, and M. G. Raizen, Phys. Rev. Lett. **76**, 4504 (1996).
 - [19] C. Sias, H. Lignier, Y. P. Singh, A. Zenesini, D. Ciampini, O. Morsch, and E. Arimondo, Phys. Rev. Lett. **100**, 040404 (2008).
 - [20] A. Eckardt, C. Weiss, and M. Holthaus, Phys. Rev. Lett. **95**, 260404 (2005).
 - [21] N. Gemelke, E. Sarajlic, Y. Bidel, S. Hong, and S. Chu, Phys. Rev. Lett. **95**, 170404 (2005).
 - [22] K. M. Hilligsøe, and K. Mølmer, Phys. Rev. A **71**, 041602 (2005).
 - [23] R. Lopes, A. Imanaliev, A. Aspect, M. Cheneau, D. B. Iron, and C. I. Westbrook, Nature **520** (2015).
 - [24] W. Zheng, and H. Zhai, Phys. Rev. A **89**, 061603 (2014).
 - [25] H. Lignier, C. Sias, D. Ciampini, Y. Singh, A. Zenesini, O. Morsch, and E. Arimondo, Phys. Rev. Lett. **99**, 220403 (2007).
 - [26] J. Struck, C. Ölschläger, M. Weinberg, P. Hauke, J. Simonet, A. Eckardt, M. Lewenstein, K. Sengstock and P. Windpassinger, Phys. Rev. Lett. **108**, 225304 (2012).
 - [27] C. V. Parker, L. C. Ha, and C. Chin, Nature Phys. **9**,

- 769-774 (2013).
- [28] S. Choudhury, and E. J. Mueller, Phys. Rev. A **90**, 013621 (2014).
- [29] C. Sträter, and A. Eckardt, Phys. Rev. A **91**, 053602 (2015).
- [30] A. Iucci, M. A. Cazalilla, A. F. Ho, and T. Giamarchi, Phys. Rev. A **73**, 041608 (2006).
- [31] P. I. Schneider, and A. Saenz, Phys. Rev. A **85**, 050304 (2012).
- [32] O. E. Alon, A. I. Streltsov, and L. S. Cederbaum, J. Chem. Phys. **127**, 154103 (2007).
- [33] O. E. Alon, A. I. Streltsov, and L. S. Cederbaum, Phys. Rev. A **77**, 033613 (2008).
- [34] J. I. Kim, V. S. Melezhik, and P. Schmelcher, Phys. Rev. Lett. **97**, 193203 (2006).
- [35] P. Giannakeas, F. K. Diakonov, and P. Schmelcher, Phys. Rev. A **86**, 042703 (2012).
- [36] S. I. Mistakidis, L. Cao, and P. Schmelcher, J. Phys. B: At. Mol. Opt. Phys. **47**, 225303 (2014).
- [37] S. I. Mistakidis, L. Cao, and P. Schmelcher, Phys. Rev. A **91**, 033611 (2014).
- [38] T. Gorin, T. Prosen, T. H. Seligman, and M. Žnidarič, Phys. Rep. **435**, 33 (2006).
- [39] D.J. Tannor, *Introduction to Quantum Mechanics: A Time-Dependent Perspective*, (University Science Books, Sausalito, California, 2007).
- [40] M. Grifoni and P. Hänggi, Phys. Rep. **304**, 229-354 (1998).
- [41] T. Wulf, C. Petri, B. Liebchen and P. Schmelcher, Phys. Rev. E **90**, 042913 (2014).
- [42] T. Wulf, B. Liebchen and P. Schmelcher, Phys. Rev. A **91**, 043628 (2015).
- [43] L. Cao, S. Krönke, O. Vendrell, and P. Schmelcher, J. Chem. Phys. **139**, 134103 (2013).
- [44] S. Krönke, L. Cao, O. Vendrell, and P. Schmelcher, New J. Phys. **15**, 063018 (2013).
- [45] A. I. Streltsov, O. E. Alon, and L. S. Cederbaum, Phys. Rev. Lett. **99**, 030402 (2007).
- [46] A. I. Streltsov, K. Sakmann, O. E. Alon, and L. S. Cederbaum, Phys. Rev. A **83**, 043604 (2011).
- [47] O. E. Alon, A. I. Streltsov, and L. S. Cederbaum, Phys. Rev. A **76**, 013611 (2007).
- [48] O. E. Alon, A. I. Streltsov, and L. S. Cederbaum, Phys. Rev. A **79**, 022503 (2009).
- [49] J. Frenkel, in Wave Mechanics 1st ed. (Clarendon Press, Oxford, 1934), pp. 423-428.
- [50] P. A. Dirac, (1930, July). Proc. Camb. Phil. Soc. (Vol. **26**, No. 03, pp. 376-385). Cambridge University Press.
- [51] J. Broeckhove, L. Lathouwers, E. Kesteloot, and P. Van Leuven, Chem. Phys. Lett. **149**, 547 (1988).